



HAL
open science

Experimental SAC305 shear stress-strain hysteresis loop construction using Hall's one-dimensional model based on strain gages measurements

Jean-Baptiste Libot, Joël Alexis, Olivier Dalverny, Lionel Arnaud, Philippe Milesi, Frédéric Dulondel

► To cite this version:

Jean-Baptiste Libot, Joël Alexis, Olivier Dalverny, Lionel Arnaud, Philippe Milesi, et al.. Experimental SAC305 shear stress-strain hysteresis loop construction using Hall's one-dimensional model based on strain gages measurements. *Journal of Electronic Packaging*, 2019, 141 (2), pp.021002-1-021002-15. 10.1115/1.4042806 . hal-02359785

HAL Id: hal-02359785

<https://hal.science/hal-02359785>

Submitted on 12 Nov 2019

HAL is a multi-disciplinary open access archive for the deposit and dissemination of scientific research documents, whether they are published or not. The documents may come from teaching and research institutions in France or abroad, or from public or private research centers.

L'archive ouverte pluridisciplinaire **HAL**, est destinée au dépôt et à la diffusion de documents scientifiques de niveau recherche, publiés ou non, émanant des établissements d'enseignement et de recherche français ou étrangers, des laboratoires publics ou privés.



Open Archive Toulouse Archive Ouverte (OATAO)

OATAO is an open access repository that collects the work of some Toulouse researchers and makes it freely available over the web where possible.

This is an author's version published in: <http://oatao.univ-toulouse.fr/22983>

Official URL: <https://doi.org/10.1115/1.4042806>

To cite this version:

Libot, Jean-Baptiste and Alexis, Joël and Dalverny, Olivier and Arnaud, Lionel and Milesi, Philippe and Dulondel, Frédéric Experimental SAC305 shear stress-strain hysteresis loop construction using Hall's one-dimensional model based on strain gages measurements. (2019) Journal of Electronic Packaging, 141 (2). 021002-1-021002-15. ISSN 1043-7398

Any correspondence concerning this service should be sent to the repository administrator:

tech-oatao@listes-diff.inp-toulouse.fr

J.-B. Libot¹

LGP,
INP/ENIT,
University of Toulouse,
47, Avenue d'Azereix,
Tarbes 65013, France;
SAFRAN Electronics and Defense,
21, Avenue du Gros Chêne,
Éragny-sur-Oise 95610, France
e-mail: jean-baptiste.libot@sfrangroup.com

J. Alexis

LGP,
INP/ENIT,
University of Toulouse,
47, Avenue d'Azereix,
Tarbes 65013, France

O. Dalverny

LGP,
INP/ENIT,
University of Toulouse,
47, Avenue d'Azereix,
Tarbes 65013, France

L. Arnaud

LGP,
INP/ENIT,
University of Toulouse,
47, Avenue d'Azereix,
Tarbes 65013, France

P. Milesi

SAFRAN Electronics and Defense,
21, Avenue du Gros Chêne,
Éragny-sur-Oise 95610, France

F. Dulondel

SAFRAN Electronics and Defense,
21, Avenue du Gros Chêne,
Éragny-sur-Oise 95610, France

Experimental SAC305 Shear Stress–Strain Hysteresis Loop Construction Using Hall's One-Dimensional Model Based on Strain Gages Measurements

Temperature-induced solder joint fatigue is a main reliability concern for aerospace and military industries whose electronic equipment used in the field is required to remain functional under harsh loadings. Due to the RoHS directive, which eventually will prevent lead from being utilized in electronic systems, there is a need for a better understanding of lead-free thermomechanical behavior when subjected to temperature variations. Characterizing solder joints properties remains a challenge as viscoplastic behavior during thermal cycling is complex, and their small dimensions prevent direct measurements from being performed. This paper reports the experimentation based on strain gage measurements, allowing the construction of the shear stress–strain hysteresis loop corresponding to Sn3.0Ag0.5Cu (SAC305) solder joints behavior during thermomechanical loading. This methodology, initially developed in 1984 by Hall for Sn60Pb40 interconnects, allows the measurement of the strain energy density dissipated during temperature cycles. Custom daisy-chained 76 I/O ceramic ball grid array (CBGA76) components were designed and assembled on flame retardant (FR-4) multilayered printed circuit boards (PCB). Four strain gages were specifically placed at the center of the assembly on top and bottom faces of both PCB and CBGA76 component. The assembly was subjected to temperature cycles and the SAC305 solder joints shear stress–strain hysteresis loop was plotted. The correlation between the measured strain energy density and measured lifetime corresponds to one point of the energy based fatigue curve for SAC305 solder joints. The hysteresis loop also provides the necessary data to derive SAC305 solder joints constitutive laws. [DOI: 10.1115/1.4042806]

Keywords: lead-free solder, hysteresis, thermal cycling, damage, microstructure

1 Introduction

Electronic equipment for aerospace and military applications can encounter a wide range of environmental stresses mainly due to thermomechanical loadings (temperature variations) eventually leading to solder joints cracking [1]. With the RoHS directive preventing the use of lead (Pb), lead-free solder joint fatigue in severe temperature environments has been widely studied among the electronic industry and academics [2]. Several fatigue models based on different fatigue criteria have therefore been developed over the years to assess solder joints durability under thermal cycling conditions [3]. Energy-based fatigue models, such as Morrow's law, are nowadays widely considered to describe lead-free solder fatigue [4]. It has indeed the advantage to take into account both strain and stress amplitudes generated during thermomechanical loading. Most studies consider an approach based

on accelerated testing and finite element modeling to calculate the strain energy density [5,6]. However, this approach requires prior knowledge of the solder material constitutive laws. Tensile, creep, and/or stress relaxation tests are therefore usually conducted in order to determine the elastic, plastic, and viscoplastic models associated with the solder material behavior. These constitutive laws are then implemented in finite element analysis software to allow accurate calculation of stress and strain within solder joints. This methodology nevertheless lacks accuracy as monotonous testing decouples viscoplastic phenomena from each other while they occur simultaneously during thermal cycling. Testing samples themselves represent another approximation as their dimensions are several orders of magnitude bigger than those from actual solder joints. Finally, the different fabrication process between test specimen and real interconnects can generate important discrepancies in terms of resulting microstructure. The accurate calculation of the strain energy density is therefore highly dependent on the prior solder material characterization. Another way to assess this damage metric and capture continuous viscoplastic effects during thermal cycles is the construction of the experimental solder joints shear stress–strain hysteresis curve

Corresponding author.

(since this curve is closed, the term “hysteresis loop” will also be used in the rest of the text). In 1984, Hall was the first to develop a methodology using relevant mechanical hypothesis and strain gages adequately placed on an electronic assembly (84 I/O leadless ceramic chip carrier (LCCC84) assembled on a flame retardant (FR-4) printed circuit boards (PCB)) to assess the shear stress and strain in Sn60Pb40 solder joints during temperature cycles [7]. The area of the loop is a measure of the cyclic strain energy per unit volume dissipated during a thermal cycle. To account for high-temperature solders, Pao et al. utilized high-temperature strain gages and beam theory assumptions to estimate the stress–strain hysteresis loop of a test specimen consisting of two beams (Al_2O_3 and Al 2024-T4, respectively) assembled with Pb90Sn10 solder joints [8]. Jih and Pao developed an analytical model to calculate shear stress and strain in Sn60Pb40 solder interconnects using Hall’s mechanical assumptions [9]. This model was then correlated with finite element analysis to provide an efficient means for modeling solder joints behavior. Clech developed an algorithm allowing the assessment of the shear stress and strain for a given solder joint assembly in order to predict its lifetime [10]. Using material properties of the LCCC84 and FR-4 PCB along with Sn60Pb40 constitutive laws, he was indeed able to fit his simulation with the experimental hysteresis loop obtained by Hall [11]. The hysteresis loop experimentation is therefore a means to evaluate thermomechanical damage in solder interconnects during thermal cycles but it is also a characterization test allowing the determination of solder materials behavior laws. This double interest is particularly interesting nowadays given that several solder material compositions are coming up on the market and since long-time accelerated testing and material characterization involve non-negligible costs for companies.

The mentioned papers report studies that have been conducted more than 25 years ago. No such test has been performed on lead-free assemblies since then. Despite its ability to capture simultaneous viscoplastic effects occurring in solder joints during thermal cycling, the precursor approach based on strain gages measurements developed by Hall is indeed complex to set up experimentally. This study describes the experimentation that has been considered to assess Sn3.0Ag0.5Cu (SAC305) thermomechanical behavior through the construction of its shear stress–strain hysteresis loop. First, a detailed description of the original work performed by Hall is given in order to explain the different hypothesis of his model necessary to understand the experimentation. Custom alumina ceramic ball grid array (CBGA76) components were designed with SAC305 solder balls located at the periphery of the package. Components were then mounted on FR-4 multilayered PCB and subjected to one reflow profile cycle. Cross sections were performed on as-reflowed SAC305 solder balls to observe their initial microstructure and ensure the representativeness of the assembled test vehicles compared to actual SAC305 interconnects. Prior to assembly, one CBGA76 component and one PCB were optically characterized to measure their respective coefficient of thermal expansion (CTE). The test assemblies were then subjected to thermal cycling between -25°C and 125°C , with a very slow ramp rate of $0.5^\circ\text{C}/\text{min}$ and 120 min dwells, until failure to determine the corresponding number of cycles to failure for a 50% failure rate ($N_{50\%}$) using Weibull distribution. Failure analysis was conducted to ensure that microstructural phenomena that usually occur on SAC305 interconnections during thermal cycling are also observed on the test vehicles. A specific CBGA76 component was instrumented with four strain gages whose resistance was monitored throughout thermal cycling. Using Hall’s equations expressing the shear stress and strain as functions of the measured strains, the hysteresis loop corresponding to SAC305 thermomechanical damage was plotted. The area of the obtained loop gives a direct measure of the strain energy density dissipated by SAC305 solder joints during thermal cycling. The correlation between this damage metric and the number of cycles to failure represents the first step to obtain a complete experimental SAC305 energy-based fatigue model.

2 Hall’s One-Dimensional model

2.1 Axial Symmetry Assumptions. In his original paper, Hall considered an axial symmetry to simplify the complex strain field generated during thermal cycling in an electronic assembly. The simplification allows the reduction to only one component for the force (radial) and the moment applied on solder joints. This assumption also excludes any out-of-plane forces and only shear forces are considered. Shear solicitations are relevant here as solder joints rarely fail due to tensile forces when subjected to thermal cycling. Figure 1 describes the forces and moments exerted by a single solder joint on a component for a real electronic assembly and for the corresponding axisymmetric model (the cylinder-shaped solder joint represented in Fig. 1 is arbitrary and does not rely on any mechanical assumption aiming to simplify calculations). The model is described for a peripheral component where solder joints are located at the edges of the package. The subscripts “c,” “s,” and “P” correspond to component, solder, and PCB, respectively, (when P is not used as a subscript, it corresponds to the component pitch). Hall’s theory also requires to know the dimensions of the assembly: distance between the critical solder joint located at the corner of the component [12] and the neutral axis “ L_D ,” the distance between each solder joint “pitch P,” thicknesses of the component “ h_c ,” the solder joint “ h_s ” and the PCB “ h_p ,” along with the elastic material properties of the component and the PCB: Young moduli “ E_c ” and “ E_p ” as well as the associated Poisson coefficients “ ν_c ” and “ ν_p ”. Based on these hypotheses, Hall derived the expressions corresponding to the

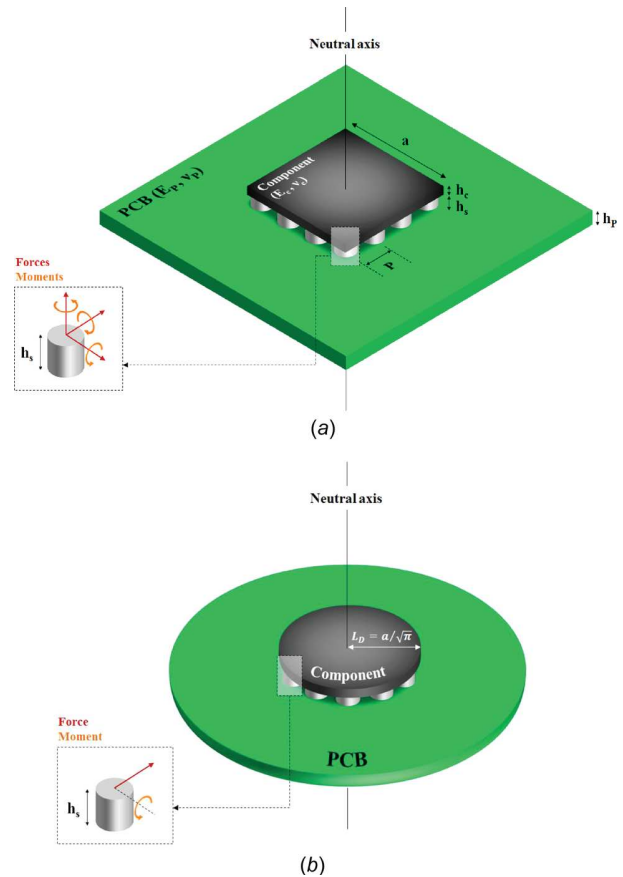


Fig. 1 Forces and moments exerted by a solder joint on component for (a) a real assembly and (b) its equivalent axisymmetric model (despite the representation, the circular PCB is assumed to behave as an infinite plate). The distance to neutral point L_D is calculated assuming the same area for the CBGA76 and its equivalent circular model.

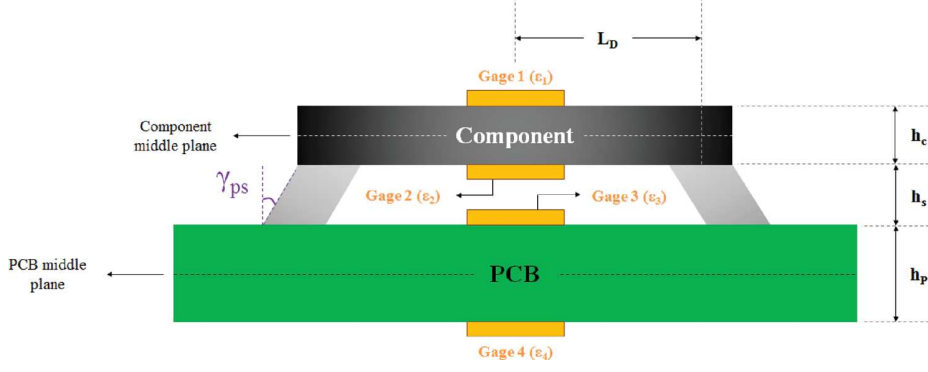


Fig. 2 Placement of the strain gages on top and bottom faces of the component and the PCB for critical solder joints shear stress and strain measurements during thermal cycling: pure shear strain situation

shear strain and stress generated in critical solder joints during temperature cycles as functions of the deformations measured by the different strain gages.

2.2 Shear Strain. The CTE mismatch between the constitutive materials of the PCB and the component drives the generation of temperature-induced shear strains within solder joints eventually leading to crack initiation and propagation causing component failure. The shear strain imposed on the critical solder joints can be divided into two contributions: pure shear and bending of the assembly. Figure 2 depicts the pure shear behavior of the electronic assembly instrumented with the four strain gages during an increase of temperature. The difference of CTE between the component and the PCB generates a shear angle at the critical solder joints which have to accommodate the thermal deformations.

When no bending is assumed, the pure shear strain can be estimated as follows:

$$\gamma_{ps} = \frac{L_D}{h_s} (\varepsilon_3 - \varepsilon_2) \quad (1)$$

Electronic assemblies are however subjected to bending under thermal cycling. This sollicitation generates another shear deformation in solder interconnects that can be evaluated assuming the same radius of curvature for the component and the PCB ($R_c = R_p = R$, i.e., $\varepsilon_2 = \varepsilon_3$) as shown in Fig. 3. Under those assumptions, Hall stated that the arcs PM and $P'M'$ were equal and that the point M was vertically above the same point on the top surface of the PCB in the flat situation.

To a first order, the generated bend angle experienced by solder joints can either be expressed according to the component or PCB strain gages measurements

$$\gamma_b = \frac{L_D}{R_c} = L_D \frac{\varepsilon_2 - \varepsilon_1}{h_c} \quad (\text{component}) \quad (2)$$

$$\gamma_b = \frac{L_D}{R_p} = L_D \frac{\varepsilon_4 - \varepsilon_3}{h_p} \quad (\text{PCB}) \quad (3)$$

As Hall utilized an FR-4 PCB and an Al_2O_3 LCCC with different flexural strengths, he knew the radii of curvature were not exactly equal and therefore defined the bend angle as their average value ($\bar{\gamma}_b$). He eventually came up with the expression of the shear strain in critical solder interconnects by combining Eqs. (1)–(3)

$$\gamma = \gamma_{ps} - \bar{\gamma}_b = \frac{L_D}{h_s} \left[\varepsilon_3 - \varepsilon_2 + \frac{h_s}{2} \left(\frac{\varepsilon_1 - \varepsilon_2}{h_c} + \frac{\varepsilon_3 - \varepsilon_4}{h_p} \right) \right] \quad (4)$$

2.3 Shear Stress. In order to obtain the shear stress generated in the critical solder joints, it is necessary to evaluate the forces

and moments exerted on peripheral interconnects when the axial symmetry hypotheses are met (uniform bending moment applied at the perimeter and a uniform radial force applied at the bottom edge of the perimeter). Figure 4 shows the shear forces and bending moments exerted by solder joints on component and PCB.

Using Newton's first law, the equilibrium conditions of the system can be written as followed:

$$F_{P/s} = -F_{c/s} = F \quad (5)$$

et

$$M'_p + M'_c = h_s F \quad (6)$$

The Roark's formulae give the curvature of the component and the PCB for an increase of temperature [13]

$$\frac{1}{R_c} = \frac{12(1 - \nu_c)}{E_c h_c^3 P} \left(M_c + \frac{F h_c}{2} \right) \quad (\text{component}) \quad (7)$$

$$\frac{1}{R_p} = \frac{6(1 - \nu_p^2)}{E_p h_p^3 P} \left(M_p + \frac{F h_p}{2} \right) \quad (\text{PCB}) \quad (8)$$

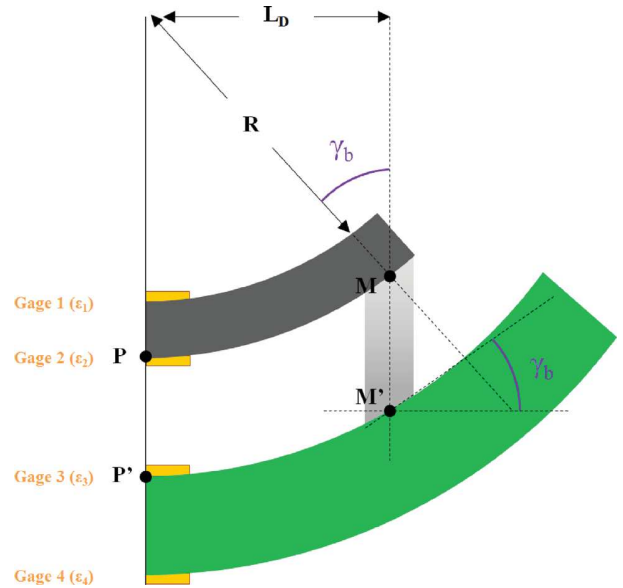


Fig. 3 Flexural behavior of the electronic assembly under thermal cycling: bend angle imposed at the critical solder joint

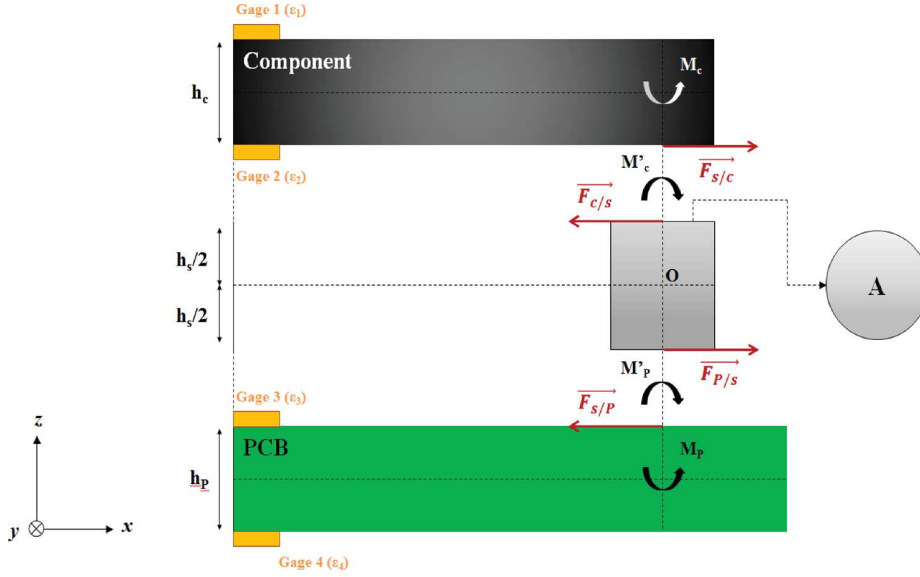


Fig. 4 Exploded view of the electronic assembly: forces and moments applied at the critical solder joint (A: contact area between the solder joint and the component assumed to represent the interfacial crack area generated during thermal cycling)

The term “ $1/P$ ” is introduced to get the moment per unit perimeter (P , the component pitch, is the distance between each joint). Equations (7) and (8) are correct assuming small deflections, which is generally the case for most electronic assemblies subjected to temperature cycles. Combining Eqs. (2) and (3), which give the expressions of the radii of curvature according to the measured strains, with Eqs. (5)–(8), the shear stress can be expressed as a function of known and measurable variables

$$\tau = \frac{F}{A} = \frac{P/A}{12 \left(h_s + \frac{h_c + h_p}{2} \right)} \left[\frac{E_c h_c^2 (\varepsilon_2 - \varepsilon_1)}{1 - \nu_c} + \frac{2E_p h_p^2 (\varepsilon_4 - \varepsilon_3)}{1 - \nu_p^2} \right] \quad (9)$$

From Eqs. (4) and (9), the shear stress–strain hysteresis loop characterizing the solder alloy thermomechanical behavior in critical interconnects can be plotted.

3 Experimental Approach

3.1 Test Vehicle for SAC305 Critical Interconnects Shear Stress–Strain Measurements

3.1.1 76 I/O Ceramic Ball Grid Array Component. The test vehicle used for the construction of the shear stress and strain hysteresis loop consists in a custom daisy-chained peripheral 76 I/O CBGA76 with 0.76 mm diameter SAC305 solder balls assembled on an FR-4 multilayered PCB. The component was designed by Kyocera (Rungis, France), and the balling process was performed by Retronix (La-Roche-Bernard, France). The CBGA76 component is a 1 mm thick, 25×25 mm package with a pitch of 1 mm. Figure 5(a) shows the scheme of the CBGA76 package with its associated dimensions. Only the inner pads were balled. The tungsten, molybdenum (W, Mo) pads are covered with Au, Ni surface finish. The alumina coat on the component bottom face is defined so that the pad opening is equal to 0.6 mm. The size of the inner pads outline is 19×19 mm. Based on Hall’s assumption stating

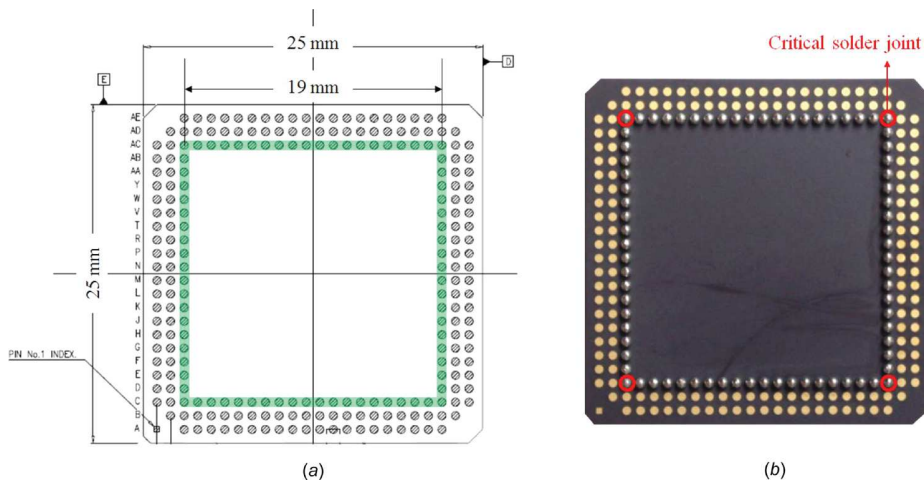


Fig. 5 (a) Outline of the custom CBGA76 component: only the inner pads are balled and (b) As-received CBGA76 component

that the component area should be equal to its corresponding circular plate area, the distance to neutral point (L_D) for the axisymmetric model is 10.7 mm. Figure 5(b) presents the custom CBGA76 with the SAC305 solder balls used for the hysteresis loop experimentation.

The critical solder joints located at the corner of the component (that is to say interconnects where fatigue cracks will occur first) are circled in red. Topography and deformation measurements were also performed in order to characterize the thermal behavior of the constitutive ceramic and determine its CTE. Tests were conducted between 25 °C and –60 °C, and from 25 °C to 150 °C. The CTE of the ceramic component is $\alpha_c = 5.5 \text{ ppm/}^\circ\text{C}$. It is worth noting that the Kyocera datasheet gives a CTE of 7.1 ppm/°C for the considered ceramic material. However, the experimental method is not specified and this value was obtained for a temperature range way beyond the thermal cycling test domain.

3.1.2 Printed Circuit Board. The PCB considered for this study is a 1.6 mm thick, 125 × 125 mm Panasonic R-1755V FR-4 with eight embedded copper layers. The introduction of the copper layers into the board structure aims to maximize its CTE and, as a result, decrease the CTE differential between the PCB and the CBGA76: $\Delta\alpha = |\alpha_p - \alpha_c|$. The board has electroless nickel immersion gold surface finish on solder mask defined pads. The conformal coating deposition is defined so that the opening on the PCB pads is equal to 0.6 mm. After reflow, the soldered balls are therefore balanced with the same “solder neck” diameters on the component and PCB sides (Fig. 6). The assumed solder crack area is thus $A = \pi \times (0.3)^2 = 0.28 \text{ mm}^2$.

In Hall’s original study, the spacing between the LCCC84 and the PCB was too small to place two gages in between (one on the bottom face of the component (i.e., gage 2) and one on the top face of the PCB (i.e., gage 3)). Hall was therefore obliged to use two assemblies where one was instrumented with gages 1, 2, and 4, and another one which was instrumented with gages 1, 3, and 4. It is worth noting that the SAC305 solder balls diameter of the CBGA76 component used here was specifically selected to ensure a sufficient standoff allowing the placement of gages 2 and 3 on one single assembly. Nevertheless, a spacing issue remains as each gage has to be wired in order to record their resistance (connection cables between the gages and the strain data acquisition system). Unlike Hall’s experimentation whose hysteresis loop was obtained using two different test vehicles, the PCB was specifically designed to get rid of this limitation and four holes were

therefore drilled underneath the component. Those holes allow the copper wires from both inside gages (2 and 3) to “go through” the PCB. This specific PCB design represents a significant improvement compared to the original experimentation from 1984 since it allows the measurement of the strain energy density on a single system. The detailed explanation of the assembly will be given in Sec. 3.3. Figure 7 shows the top and bottom of the PCB with the designed four holes and the different copper pads used for strain or component daisy-chained resistance measurements.

The PCB was also subjected to topography and deformation measurements to determine its CTE. The obtained value is $\alpha_p = 15.4 \text{ ppm/}^\circ\text{C}$. As it can be seen in Fig. 7(a), four CBGA76 components can be assembled on the PCB. Since the strain gage 3 placed on top of the PCB prevents classic stencil printing from being performed, the hysteresis loop test vehicle consists of only one CBGA76 package soldered at the location of the four holes (the assembly process is described in Sec. 3.3), while the “thermal cycling” test vehicles used to determine $N_{50\%}$ are classically assembled using four CBGA76 components. Sections 3.2–3.5 aim to describe solely the hysteresis loop test vehicle.

3.2 Strain Gages. In this study, RY96-3/350 strain gages from the company HBM were used. Those are rosette gages allowing strain measurements in three directions: 0 deg, 45 deg, and 90 deg. Since the critical solder interconnects are located in the diagonals of the assembly, only the 45 deg-steered gages are wired. The objective of the experimentation is to determine the shear stress–strain state in the critical solder joints from PCB and component strain measurements during thermal cycling. The selected strain gages were therefore calibrated with quartz material whose low CTE ($\alpha_{\text{quartz}} = 0.6 \text{ ppm/}^\circ\text{C}$) allows component and PCB thermal strain measurements. The resistive grid is 3 × 1.5 mm with an impedance of 350 Ω. Each strain gage is applied on the test assembly using M600 adhesive. The choice of the adhesive material is very important as it should resist the reflow temperature profile as well as the thermal cycling tests. The M600 adhesive polymerizes at 80 °C during 4 h and can be used for temperatures ranging from –269 °C to 370 °C [14]. Prior to gage application, it is necessary to prepare the PCB and CBGA76 surfaces to ensure a good bonding. Thus, conformal coating from the PCB was locally removed and the surface was then abraded. The constitutive ceramic material of the component does not allow hand abrasion and a sandblasting process was therefore applied to roughen the alumina surface. The order of magnitude for the deformations measured by these strain gages is typically around 10^{-6} . Strain gages must therefore be able to detect very small resistance changes during thermal cycling. To account for this sensitivity, each strain gage is configured in Wheatstone bridge circuits. Since strain measurements are computed from resistance variations, it is also necessary to perform 4-wire resistance measurements to get rid of the wires resistivity. The connection path between the strain gage and the HBM acquisition data system is divided into three parts:

- Enameled copper wire (0.05 mm diameter).
- Copper traces defined during the PCB design phase.
- Connection cables between the PCB and the HBM data acquisition system.

The first step is the most complex and probably the most important as it cannot be redone after assembly. It indeed consists in soldering very thin enameled copper wires to the leads of strain gages 2 and 3 (inside gages between the PCB and the CBGA76 component) and make them go through the PCB holes to further solder them on copper pads located on the PCB bottom. Hand soldering of the Cu wires is typically performed using classic tin-lead solder. However, a lead-free SAC305 process with a higher melting temperature is considered in this study. A nonconvenient high-Pb content solder alloy has therefore to be used (5.0Sn-93.5Pb-1.5Ag). Figure 8 shows the bottom of the PCB with the instrumented strain gages after assembly.

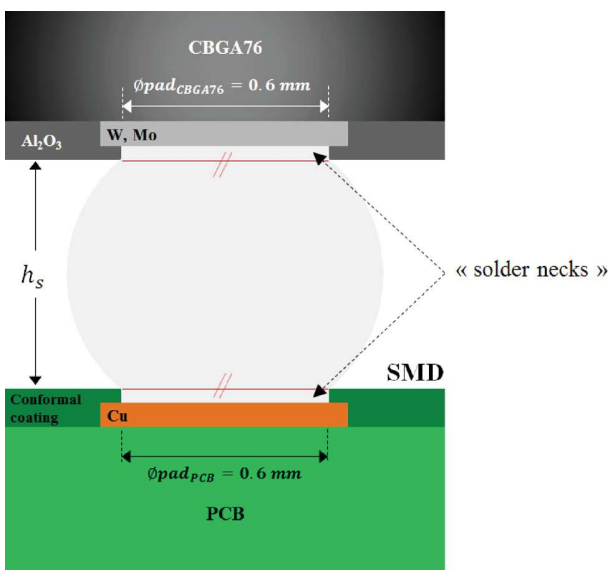


Fig. 6 Schematic representation of an assembled solder ball with the balanced sections on PCB and CBGA76 sides

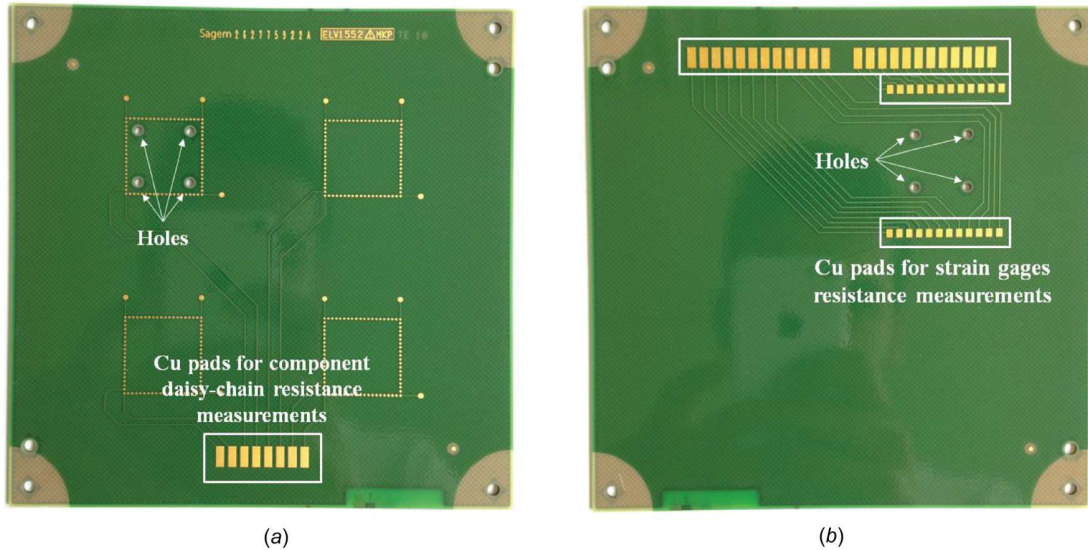


Fig. 7 (a) Top and (b) bottom faces of the PCB

3.3 Assembly Procedure. The assembly process for the hysteresis loop test vehicle is specific as it has to be subjected to a reflow temperature profile, whereas strain gages on the CBGA76 component and the PCB prevent classic stencil printing and package deposit on solder paste from being conducted. A manual phase aiming to pre-assemble the CBGA76 and the PCB has therefore to be performed prior to reflow soldering. The first step is to manually stencil print the PCB to deposit a sufficient volume of solder paste on copper pads. Once this step is achieved, the CBGA76 component has to be placed on the PCB. However, strain gage 2 placed on the component bottom has free enameled copper wires that has to go through the PCB holes. As a result, enameled copper wires from this strain gage were specifically folded so that the 90 deg folds are orthogonally facing the PCB holes during the pre-assembly process. Figure 9 presents the modified stencil screen used for SAC305 solder paste deposit and the instrumented CBGA76 component showing the folding of the enameled copper wires from gage 2.

The pre-assembly process is conducted using a Zevac rework station, which allows the accurate placement of the CBGA76 component on its PCB. A system based on the use of a camera and a beam splitter is utilized to align the solder balls with the corresponding PCB copper pads. Once this alignment is set, the CBGA76 component vertically goes down and the enameled

copper wires can easily go through the PCB, thanks to the 90 deg folds orthogonally facing the holes. A slight pressure is applied when the component is on the PCB to ensure a good prebonding before reflow soldering. Figure 10 shows the pre-assembly experimental setup along with a schematic of its principle.

After pre-assembly, the hysteresis loop test vehicle is placed in the reflow oven for final soldering. The corresponding SAC305 reflow profile was previously determined using thermocouples placed on the test assembly. Binocular visual inspections along with X-ray analysis (RX) analysis are performed in order to identify any assembly defects such as solder balls bridging. Figure 11 presents the reflow temperature profile considered in this study, as well as the final hysteresis loop test vehicle and the RX analysis showing no solder ball defects.

3.4 Solder Joints Microstructure. Resistance to creep deformation depends on solder joint's microstructure [15]. Identifying the microstructure is therefore necessary to understand thermal cycling-induced damage in SAC305 interconnections. After reflow soldering, it is necessary to perform cross section and optical microscopy observations to ensure the obtained SAC305 solder balls present the classically observed dendritic microstructure (β -Sn dendrites + interdendritic Ag_3Sn intermetallic compound

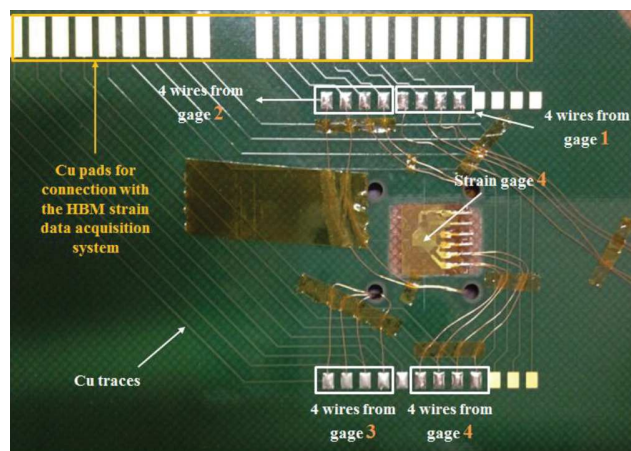


Fig. 8 Printed circuit board's bottom after assembly: strain gages wiring with 0.05 mm diameter enameled Cu wires

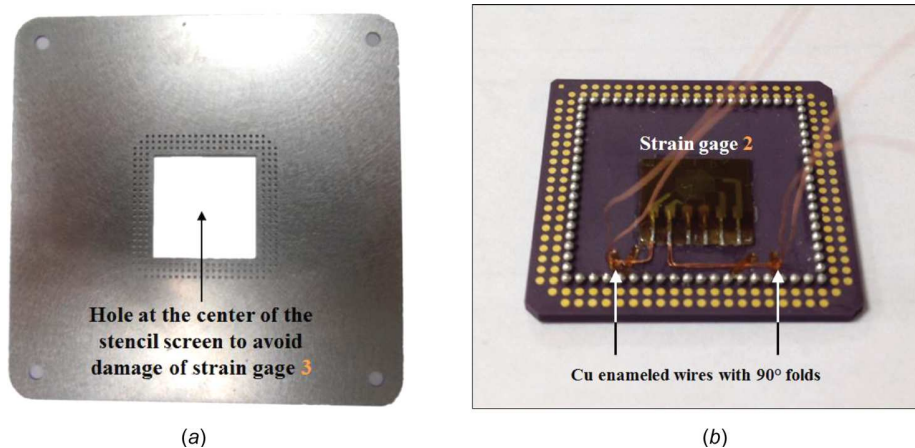


Fig. 9 (a) 130 μm custom stencil screen and (b) folded enameled copper wires from strain gage 2

(IMC) along with macrograin and interlaced morphologies [16]. It is also important to verify whether the IMC formed at the PCB interface is thick enough to ensure a good mechanical bonding while avoiding potential brittle cracks. Figure 12 shows micrographs of a single as-solidified SAC305 solder ball observed under normal and polarized light, as well as a micrograph showing the $(\text{Cu,Ni})_6\text{Sn}_5$ IMC layer formed at the interface between solder joint and the PCB pad. Every observed solidified solder ball depicts a β -Sn dendritic microstructure along with macrograins morphology. Moreover, smaller interlaced grains are locally observed on some interconnects as it is sometimes observed on typical as-reflowed SAC305 solder joints. The measured IMC layer thickness is $2.5 \pm 0.8 \mu\text{m}$, which is consistent with values found in the literature [17].

3.5 Thermal Cycling Test. The hysteresis loop test vehicle is then placed in a thermal chamber and connected to the HBM data acquisition system converting the gages resistance measurements into strain values. The temperature cycle applied lasts 14 h:

- Temperature excursion: -25°C – 125°C .
- Ramp rate: $0.5^\circ\text{C}/\text{min}$.
- Dwell time: 120 min.

As it was previously stated by Hall in his original paper, thermal ramps have to be slow so that viscoplastic phenomena (creep

and stress relaxation) can occur. This very slow kinetics also avoids potential temperature gradients within the assembly due to different thermal inertias between the CBGA76 component and the PCB. Computing Eqs. (4) and (9) with the measured strains, shear stress and strain in the critical SAC305 solder joints can be obtained. Figure 13 shows the experimental setup considered for the SAC305 shear stress–strain hysteresis loop construction.

In parallel, temperature cycling test is performed on classically reflow-soldered test assemblies (thermal cycling test vehicles with four mounted CBGA76 components) in order to determine the number of cycles to failure for a 50% failure rate ($N_{50\%}$). Three thermal cycling test assemblies representing 10 CBGA76 components are therefore monitored to assess SAC305 thermomechanical durability (two boards with four components and one board with only two components). The failure criterion is based on the 20% resistance increase for five consecutive scans according to the IPC-9701A standard [18].

4 Results and Discussion

4.1 SAC305 Shear Stress–Strain Hysteresis Loop. Viscoplastic phenomena are believed to occur when $T_H = T/T_m > 0.4$ (T_H is the homologous temperature defined as the ratio between the temperature and the melting temperature of the material T_m) [19]. Between -25°C and 125°C , SAC305 homologous

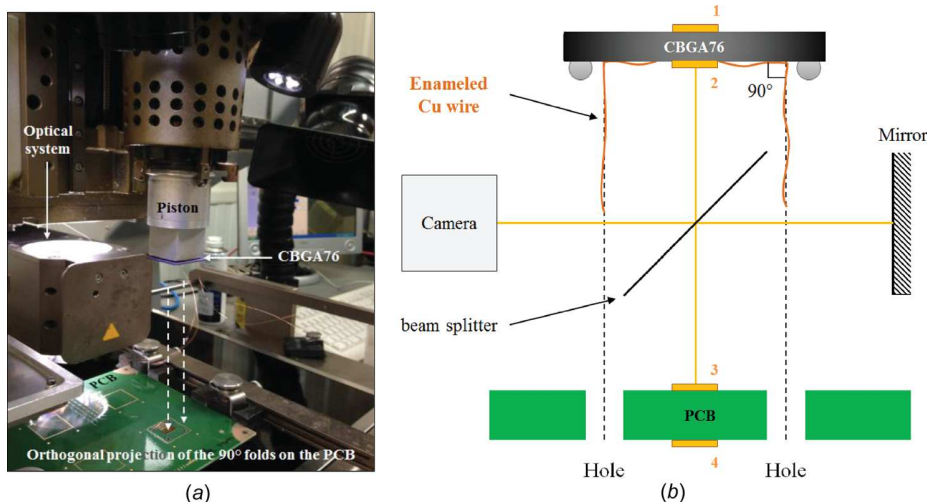
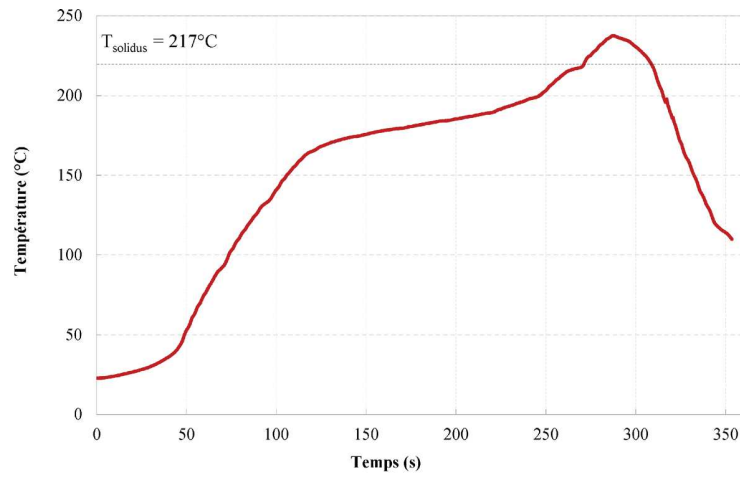


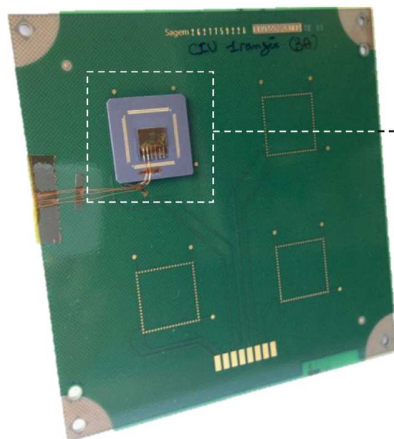
Fig. 10 (a) Experimental setup for the pre-assembly of the CBGA76 component on the PCB and (b) pre-assembly principle

temperatures are, respectively, close 0.5 and 0.8. In this homologous temperature range, the time-dependent material response, that is to say creep and stress relaxation of SAC305 solder alloy, is significant and thermal cycling-induced viscoplastic effects can therefore be seen from shear stress and strain data collected with strain gages. Figure 14 shows the temporal evolution of shear stress and strain during three consecutive temperature cycles (strain gages data were recorded every 50 s). The negative stress developed at the early stage of thermal cycling is due to the experimental configuration. The thermal chamber was indeed set up to stabilize the temperature at 20 °C for 10 min prior to temperature cycling between -25 °C and 125 °C. Since room temperature was around 25 °C, the decrease of temperature to reach 20 °C lead to this initial negative shear stress. It can be seen that stress relaxation and creep occur throughout the entire thermal cycles. During ramp-up of the first cycle, the shear stress increases and reaches a maximum value around 85 °C indicating that SAC305 solder material becomes less resistant to the increasing thermal deformations. Between 85 °C and 125 °C, the ductility of the solder joint increases and, since the ramp rate is very slow, stress decreases through a relaxation mechanism. This effect is only observed for the first cycle while the maximum stress values at the second and third cycles are reached when $T = 125$ °C. During dwell time at high temperature, a thermal deformation is imposed and it is clear that stress relaxation occurs with a stress release of about 42.5%

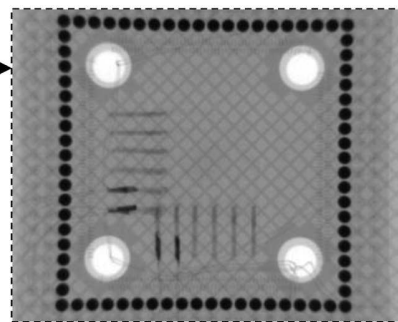
after 120 min for the first cycle. The second and third hot dwells depict a stress reduction around 32%. During the ramp down between 125 °C and -25 °C, shear stress significantly increases as solder joint becomes more and more resistant to creep deformations. Absolute maximum stress values reached at -25 °C oscillate around 25 MPa. In spite of these high stresses, stress relaxation occurring at cold dwells is less significant than hot dwell relaxations because the viscoplastic contributions are less significant when the homologous temperature is close to 0.4 ($T_H = 0.5$ at -25 °C). Only 5.2% of the absolute maximum stress is hence relaxed. Whether it is at hot or cold temperature, stress relaxation proceeds at the fastest rate at the beginning of dwell times. The inelastic shear strain driven by the CTE mismatch between the CBGA76 component and the PCB is also visible throughout thermal cycles. During ramp-up, shear strain increases to reach a maximum value of 1.75×10^{-2} . At hot dwells, viscoplastic effects are dominant and creep strains increase as well as stress relaxation occurs. When temperature decreases between 125 °C and -25 °C, shear angle becomes negative at -4 °C and reached a maximum absolute value of 3.2×10^{-3} . Even though viscoplastic phenomena are not as dominant as they are at high temperature, shear strain increases during cold dwells. It is also worth noting that creep strain rates are temperature-dependent. During ramp-up between -25 °C and 125 °C, the shear strain rate progressively increases as the temperature increases



(a)



(b)



(c)

Fig. 11 (a) SAC305 reflow temperature profile, (b) final hysteresis loop test vehicle, and (c) RX analysis performed on the assembled test vehicle. The shear stress–strain in the critical solder joints is assumed to be the same regardless of the number of assembled components (no influence of the adjacent CBGA76).

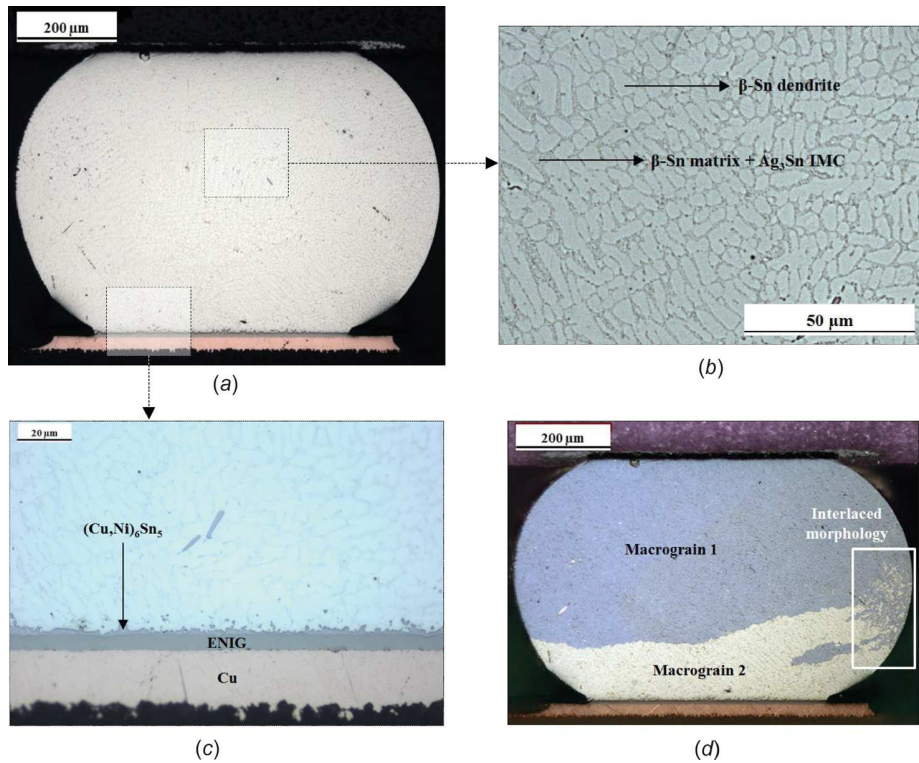


Fig. 12 Microstructure and β -Sn grains morphologies of the obtained SAC305 solder joints: (a) Micrograph of an as-reflowed solder ball under normal light, (b) close-up showing the dendritic microstructure along with the Ag_3Sn IMC in the interdendritic spaces, (c) micrograph showing the interfacial $(\text{Cu,Ni})_6\text{Sn}_5$ IMC layer, and (d) micrograph of the as-solidified SAC305 solder ball observed under polarized light showing the macrograins and interlaced morphologies

(i.e., for $i = 1, 2, 3$: $(d\gamma/dt)_{\text{cold}, i} < (d\gamma/dt)_{\text{ramp-up}, i}$), that is to say the viscoplastic contributions become more and more significant. During the ramp-down from 125°C to -25°C , the inelastic shear strain rate remains constant. From shear strain and stress temporal evolutions, it is interesting to see that there is stabilization from the second thermal cycle with constant measured maximum shear and strain values.

For each time increment, shear stress can then be expressed as a function of the shear strain, and the SAC305 hysteresis loops are thus obtained by cross-plotting Figs. 14(a), 14(b), and 15(a). Hall's hysteresis loop corresponding to Sn60Pb40 solder alloy is also given for qualitative comparison (Fig. 15(b)). The shape of

the loops illustrates the highly nonlinear, time, and temperature-dependent behavior of SAC305 solder interconnects subjected to thermomechanical loading. First, it is interesting to notice that the obtained loop is comparable to Hall's hysteresis curve in terms of shape. However, contrary to Hall's hysteresis loop whose Sn60Pb40 solder joints stress reduction was almost complete prior to hot dwells, shear stress in SAC305 solder balls do not totally relax between -25°C and 125°C . Significant stress reduction is therefore observed during the 120 min dwell at 125°C . It is also interesting to point out that, unlike Sn60Pb40 solder joints whose shear strain remains constant between -25°C and 30°C , shear strain in SAC305 interconnects depicts a linear evolution during

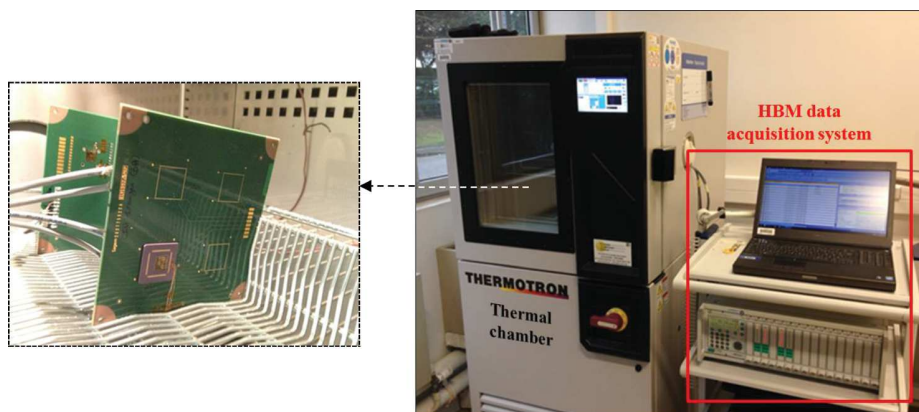


Fig. 13 Hysteresis loop experimental setup

the first part of the ramp-up between $-25\text{ }^{\circ}\text{C}$ and $125\text{ }^{\circ}\text{C}$. This could mean that SAC305 elastic contribution is negligible compared to the viscoplastic effects involved during thermal cycling.

As it was observed with the temporal evolutions of shear stress and strain, the hysteresis loops tend to stabilize after three thermal cycles. Figure 15(b) also shows isotherm lines whose slope is “ $-\kappa$.” Those have been introduced by Hall [20] and are called “lines of isothermal reduction” or “stress reduction lines.” The corresponding equation can be written as follows:

$$\gamma + \frac{\tau}{\kappa} = \frac{L_D |\Delta\alpha| (T - T_0)}{h_s} \quad (10)$$

where T_0 is the “reference temperature,” often considered as the ambient temperature. At this temperature, shear stress and strain are assumed to be equal to zero. This assumption is believed to be correct for this study because time between assembly process and

thermal cycling test was long enough to ensure stress relaxation in solder joints. Equation (10) gives the fundamental relationship between shear stress τ and strain γ at current temperature T . Clech stated that this formulation shows that the thermal expansion differential between the PCB and the mounted component (right side of Eq. (10)) is accommodated by Ref. [11]:

- Shear deformation of the solder joints (γ).
- And elastic deformations of the PCB and the component (τ/κ).

The parameter κ of the stress reduction lines has a physical meaning as it is a function of the assembly stiffness K . Based on the axisymmetric model assumptions, κ can be expressed as follows:

$$\kappa = \frac{K \cdot h_s}{A} \quad (11)$$

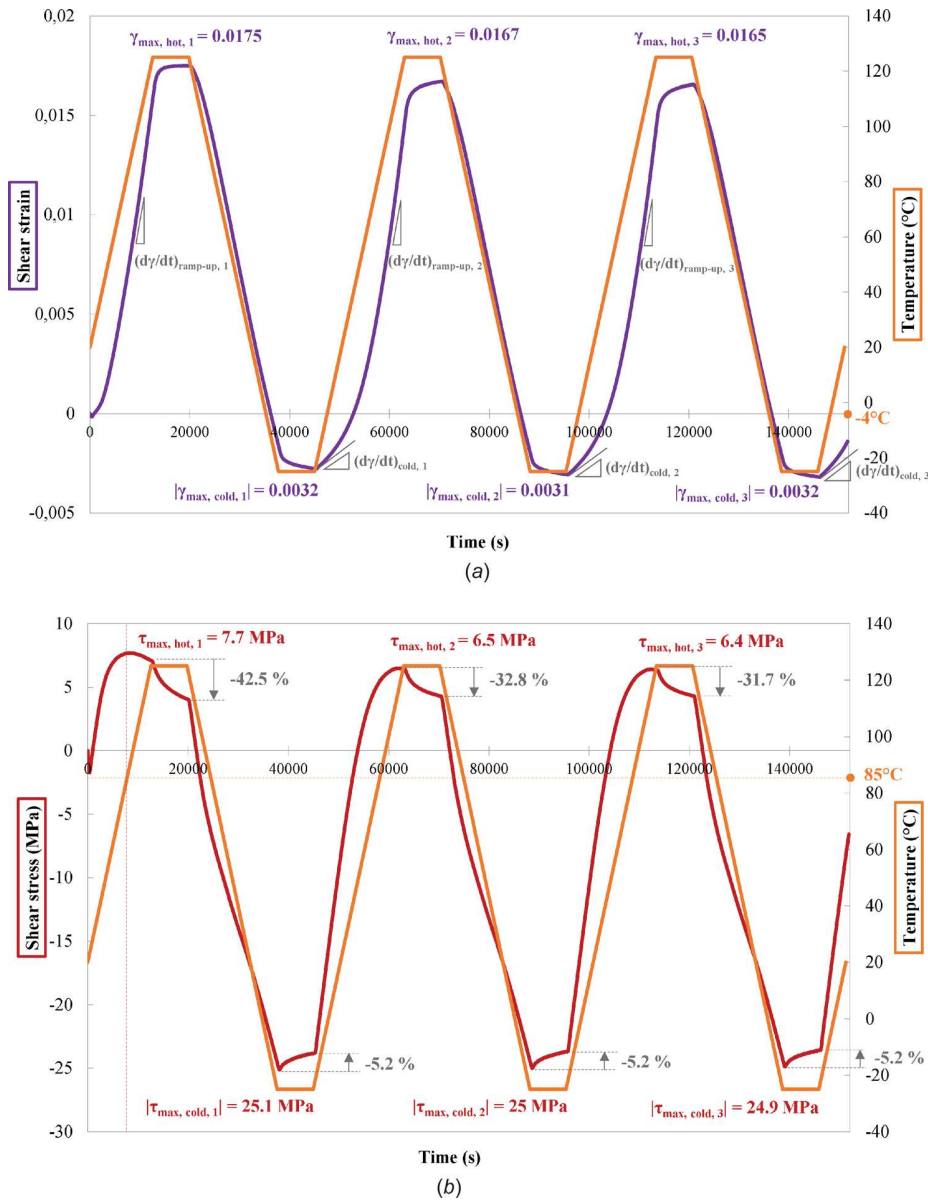


Fig. 14 Temporal evolution of shear (a) strain and (b) stress measured with the four strain gages during thermal cycling

with

$$K = \frac{P}{L_D} \left(\frac{1 - \nu_p^2}{2E_p h_p} + \frac{1 - \nu_c}{E_c h_c} + \frac{H^2}{\frac{E_c h_c^3}{12(1 - \nu_c)} + \frac{E_p h_p^3}{6(1 - \nu_p^2)}} \right)^{-1} \quad (12)$$

where $H = h_c/2 + h_s + h_p/2$. Every term of Eqs. (11) and (12) is known, and the stiffness parameter can therefore be numerically determined. Figure 16 shows the stabilized SAC305 shear stress–strain hysteresis loop with its corresponding isothermal stress reduction lines at -25°C , -10°C , 0°C , 25°C , 50°C , 75°C , 100°C , and 125°C . It is interesting to notice that experimental stress reduction lines seem parallel with each other.

To ensure Hall’s hypotheses are validated, a comparison between the experimental slopes and the theoretical value

extracted from Eqs. (11) and (12) is conducted. Table 1 gives the numerical values of the CBGA76 and PCB material properties as well as the dimensions of the assembly.

Theoretical value of κ :

$$\begin{aligned} \kappa_{\text{theoretical}} &= \frac{(1 \times 0.5)/(10.7 \times 0.28)}{\frac{1 - 0.3^2}{2 \times 24,218 \times 1.6} + \frac{1 - 0.2}{310,000 \times 1} + \frac{1.8^2}{\frac{310,000 \times 1^3}{12(1 - 0.2)} + \frac{24,218 \times 1.6^3}{6(1 - 0.3^2)}}} \\ &\approx 1957 \text{ MPa} \end{aligned}$$

The absolute values of the measured slopes at -25°C and 125°C , are, respectively, 2073 MPa and 1760 MPa (for both linear

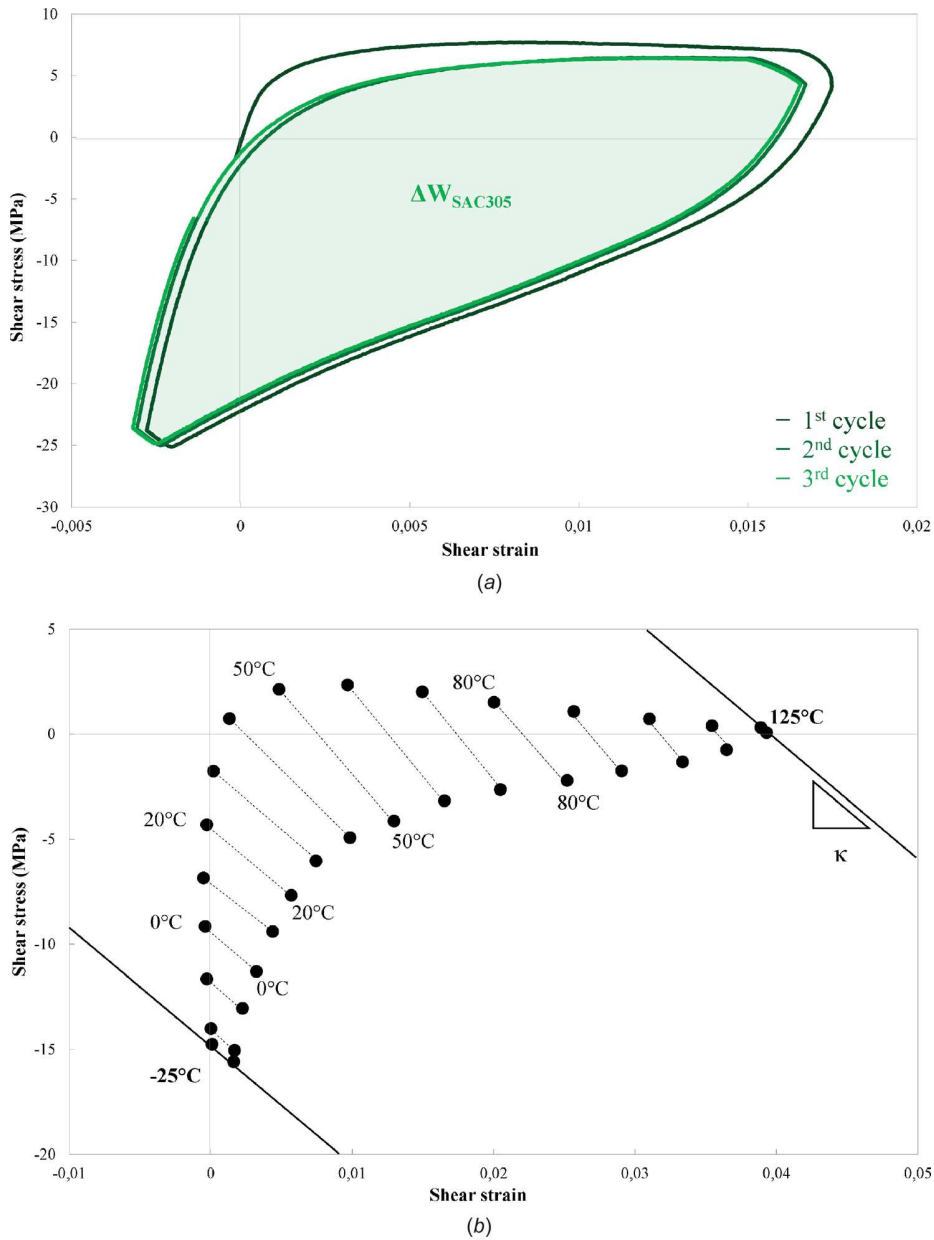


Fig. 15 (a) Measured SAC305 solder joint shear stress–strain hysteresis loops for three thermal cycles between -25°C and 125°C with $0.5^\circ\text{C}/\text{min}$ ramps and 120 min dwell (the graph depicts raw data and no smoothing has been performed) and (b) Experimental Sn60Pb40 solder joint shear stress–strain hysteresis loop obtained by Hall [7]

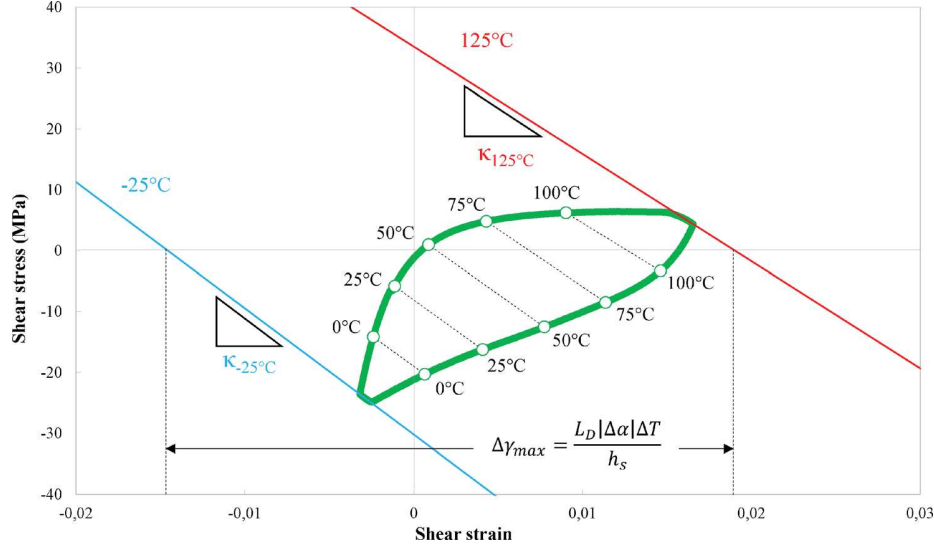


Fig. 16 Stabilized SAC305 shear ($\tau - \gamma$) hysteresis loop with its corresponding stress reduction lines

regressions, $R^2 = 0.996$). This differential can be explained with the temperature-dependent material properties of the PCB and the component that have not been taken into account to determine the shear stress (Eq. (9)). As materials usually get stiffer at low temperature, it is not surprising to find out a higher value for the stiffness parameter at -25°C . As a consequence, it is consistent that the theoretical stiffness parameter is in between the extreme values determined at -25°C and 125°C :

$$\kappa_{125^\circ\text{C}} < \kappa_{\text{theoretical}} < \kappa_{-25^\circ\text{C}}$$

Material properties of the PCB and the CBGA76 component have been assessed at ambient temperature (25°C). The stiffness parameter measured at this specific temperature should therefore be close to the theoretical value of 1957 MPa. In fact, a very small difference of 2% is found since the slope of the stress reduction line at 25°C is $\kappa_{25^\circ\text{C}} = 1996 \text{ MPa}$. This first verification based on experimental and calculated stiffness parameter values allows the validation of Hall's model hypotheses.

Another way to bear out the one-dimensional (1D) model's hypotheses relies on the determination of the differential of CTE between the CBGA component and the PCB. The stress reduction lines at -25°C and 125°C intersect the x -axis in two coordinates whose difference is the maximum shear strain amplitude imposed on critical solder joints (i.e., shear strain if the interconnects were totally accommodating). It corresponds to the right term of Eq. (10)

$$\Delta\gamma_{\text{max}} = \frac{L_D |\Delta\alpha| (T - T_0)}{h_s} \quad (13)$$

The only unknown in this equation is the CTE mismatch between the CBGA76 component and the PCB $\Delta\alpha$ whose value can therefore be easily determined (the subscript "model" is used to

differentiate CTE mismatches determined with the hysteresis loop measurement and thanks to the optical characterization, which will be subscripted "experimental"). As a reminder, the experimental CTE of the CBGA76 and the PCB are $5.5 \text{ ppm}/^\circ\text{C}$ and $15.4 \text{ ppm}/^\circ\text{C}$, respectively. The experimental CTE mismatch is therefore $\Delta\alpha_{\text{experimental}} = 10.2 \text{ ppm}/^\circ\text{C}$.

Calculation of $\Delta\alpha_{\text{model}}$:

$$\Delta\alpha_{\text{model}} = \frac{\Delta\gamma_{\text{max}} h_b}{L_D \Delta T} = \frac{0.034 \times 0.5}{10.7 \times [125 - (-25)]} = 10.6 \text{ ppm}/^\circ\text{C}$$

The CTE differential found with the experimental SAC305 hysteresis loop is very close to the measured value determined through optical analysis (only 4% difference). Hence, this second verification confirms Hall's hysteresis loop model.

Shear strain-stress hysteresis loop is a representation of the thermomechanical damage accumulating in critical solder joints during thermal cycling. The area of the loop indeed gives an experimental value of the strain energy density per cycle ΔW . This damage metric has the dimension of energy per unit volume and can be used as a fatigue criterion in energy-based solder fatigue models. From the measured SAC305 shear strain-stress hysteresis loop, the experimental strain energy density per cycle is $\Delta W_{\text{SAC305}} = 0.3 \text{ mJ}/\text{mm}^3$. In this study, reproducibility of the experimentation was ensured with a second assembly, which gave a strain energy density of $0.3 \text{ mJ}/\text{mm}^3$ as well. For clarity purpose, however, this hysteresis loop was not included in the publication. A shift toward the high stress values was indeed observed for this hysteresis loop, which is not consistent with SAC305 solder joints thermomechanical behavior (absolute value of shear stress must be higher at low temperature than at high temperature). Nevertheless, the stress range, strain range, and shape of the loops were virtually identical, therefore leading to the same strain energy density. An assumption based on stress relaxation occurring at

Table 1 Material properties and dimensions of the hysteresis loop test assembly

Assembly		Solder		PCB			CBGA76		
L_D	P	A	h_s	E_P	h_P	ν_P	E_c	ν_c	h_c
mm	mm	mm^2	mm	MPa	mm	N/A	MPa	N/A	mm
10.7	1	0.28	0.5	24,218	1.6	0.3	310,000	0.2	1

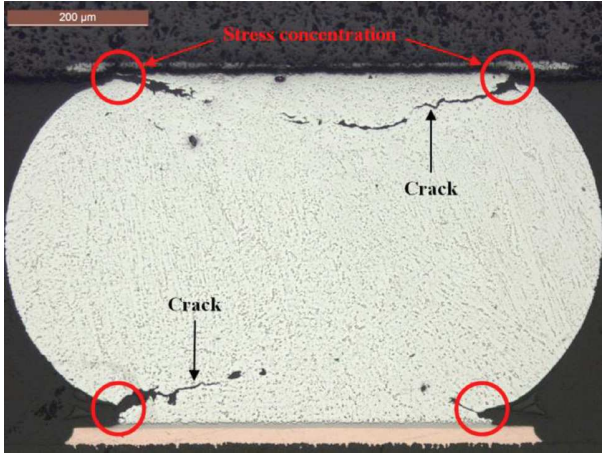


Fig. 17 Failed solder ball presenting partial cracks on component and PCB sides

ambient temperature was made to explain this phenomenon. The hysteresis loop presented in Fig. 15(a) was indeed plotted several months after assembly, whereas the other one was plotted one week after solder reflow. Further work will be conducted with new test assemblies for which a thermal treatment will be conducted after reflow to release initial stress in solder joints. Correlating ΔW_{SAC305} with an associated number of cycles to failure ($N_{1\%}$) would provide a first point for the construction of a one-dimensional experimental SAC305 energy-based fatigue curve. Three-dimensional (3D)-FEM is ongoing to model the experimentation and fit the surface deformations of the CBGA76 and the PCB (where the strain gages are placed) with the experimental data recorded by the strain gages (that is to say, fit the numerical hysteresis loop with the experimental one). A transfer function between the experimental one-dimensional hysteresis loop and the calculated 3D strain energy density dissipated in the damaged volume of the corner balls could therefore be determined. This would eventually allow the determination of a fatigue curve that could be used for durability evaluation of 3D ball grid array assemblies.

4.2 Failure Analysis. Cross sections were performed in order to identify the failure mode generated during thermal cycling. One row of interconnections was analyzed representing 20 solder interconnections. Every ball was totally or partially cracked. There is a stress gradient in the row due to the varying distance to neutral point for each interconnection. Total cracks are mainly observed at corners of the component, which confirms the critical solder balls location (Fig. 5(b)). It is also interesting to notice that the balanced sections of the solder balls (Fig. 6) allow crack initiation and propagation on component side as well as PCB side.

Figure 17 shows a micrograph of a cracked solder ball presenting damage in the high strain areas on component and PCB sides. Cracks initiate at the solder necks where stress concentration is important and propagate along each side.

A more in-depth analysis was performed under white and polarized light in order to observe the microstructure evolutions due to temperature cycling (Fig. 18). It is interesting to notice that Ag_3Sn coalescence occurred along the crack path leading to the loss of the dendritic structure. This IMC coarsening is commonly observed on damaged SAC305 interconnections after temperature cycling [21]. The evolution of the IMC dimensions throughout thermal cycling is believed to induce a change in creep resistance since Ag_3Sn precipitates in as-reflowed solder joints act as obstacles for dislocation motion. The observation of the same cross section under polarized light reveals recrystallized β -Sn grains near the fatigue crack. Recrystallization is also a common phenomenon observed on SAC305 solder joints after thermomechanical damage [22]. Failure analysis performed on failed CBGA76 component showed that the corresponding failure mode and microstructural evolutions are representatives of those usually observed on SAC305 solder joints. It is also worth noting that plotting the shear stress–strain hysteresis loop continuously throughout thermal cycling would potentially show an evolution in the loop shape that could capture these microstructural changes.

4.3 Thermomechanical Durability Results. Thermal cycling test was conducted until failure of nine assemblies (one assembly failed due to infant mortality) in order to obtain the statistical distribution of the number of cycles to failure using Weibull analysis (Fig. 19). It is important to note that those test assemblies were not instrumented with strain gages as the only purpose here was to measure the number of cycles to failure.

For critical applications, a low failure rate should be considered to assess thermomechanical durability of SAC305 solder joints. The number of cycle to failure for 1% failure rate ($N_{1\%}$) is therefore determined from the Weibull distribution. The correlation between the cyclic strain energy density determined with the hysteresis loop and these lifetime data signifies that when 0.3 mJ/mm^3 of the cyclic strain energy density is dissipated in SAC305 solder joints, 1% of the corresponding assemblies population will fail after $N_{1\%} = 73$ cycles.

Thermomechanical durability of electronic assemblies can be estimated using energy-based models such as Morrow's law

$$\Delta W = K(N)^c \quad (14)$$

where K and c are the constants depending on solder material. In the current advancement of this study, collected data are not sufficient to derive the material-dependent parameters K and c for SAC305 solder alloy. Nevertheless, performing thermal cycles with different temperature amplitudes would provide other

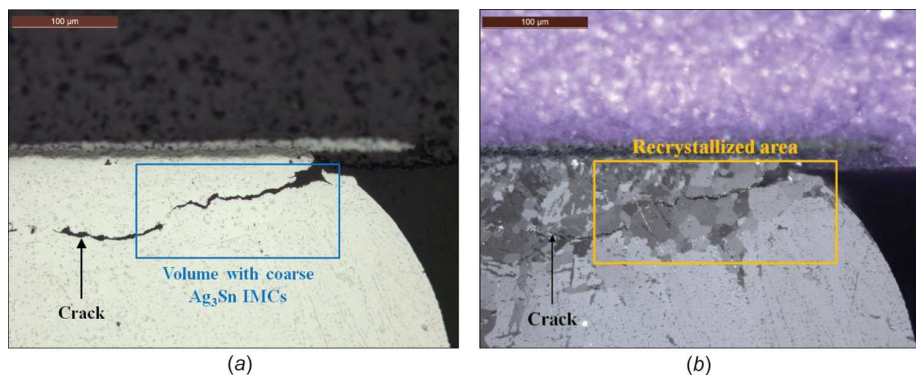


Fig. 18 Solder crack on component side observed under (a) white and (b) polarized light

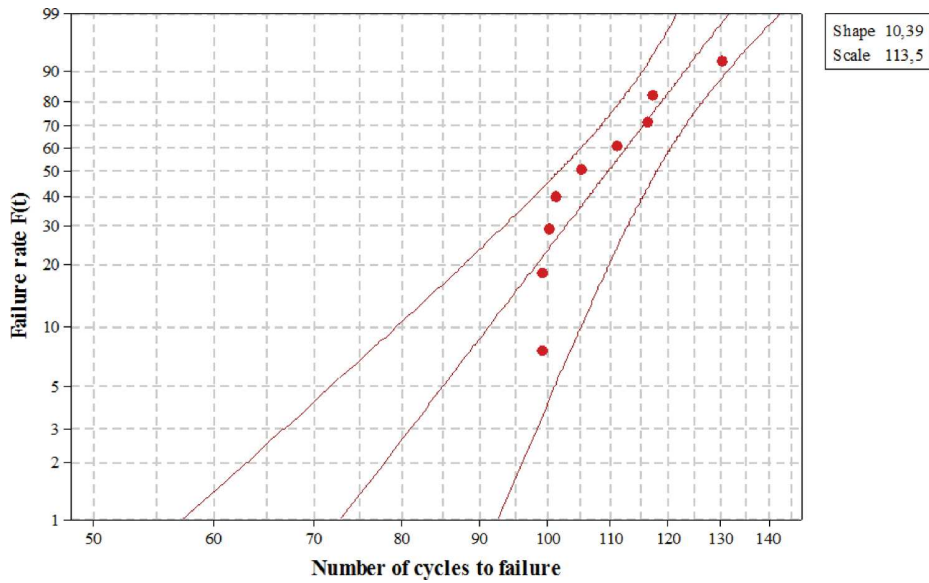


Fig. 19 Weibull plot corresponding to the failed CBGA76 components

doublets ($\Delta W, N_{1\%}$) that could allow a power law regression leading to the determination of K and c . As a result, hysteresis loop can potentially be a very powerful tool to assess thermomechanical fatigue of solder joints.

Another important advantage of the developed methodology also relies on the fact that it can be considered as a characterization test. Hysteresis loop can indeed be used as a mean to determine complex solder material behavior during temperature cycling. Using nonlinear curve fitting techniques coupled with

FEM analysis (modeling of the hysteresis loop test assembly), constitutive laws (elastic, plastic, and viscoplastic) for SAC305 solder joints could be derived. For example, the Anand model, which is a well-known unified viscoelastic law for solder alloys [23], could be determined. These material models can then be implemented in FEM software to accurately calculate stress and strain in SAC305 solder interconnects. Once the curve fitting would be achieved, a transfer function correlating the experimental strain energy density (area of the loop = ΔW_{Exp}) and the

« Hysteresis loop » test vehicle

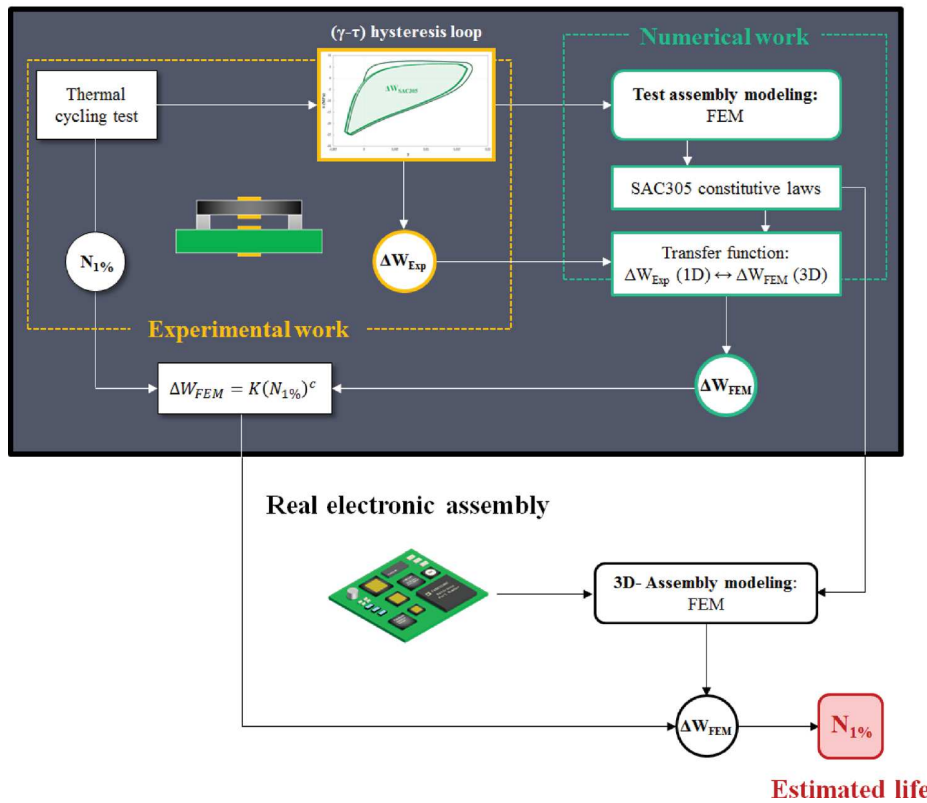


Fig. 20 Chart describing the methodology to follow in order to accurately assess SAC305 solder joints durability

calculated strain energy density dissipated in the damage volume (identified as the recrystallized area) of the critical solder joint (ΔW_{FEM}) could indeed be determined. A fatigue model based on this energy-based criterion could therefore be derived. For a given assembly subjected to a specific temperature cycle, the determination of the numerical cyclic strain energy density in the critical solder ball could therefore be correlated to this thermomechanical fatigue model to estimate its lifetime. Figure 20 presents the ideal methodology that should be considered in order assess thermal cycling durability of SAC305 electronic assemblies. While the overall procedure has been employed in the literature [24–27], the preliminary steps encompassing the determination of the experimental hysteresis loop and the material characterization are essential to improve the durability assessment of SAC305 solder joints.

5 Conclusions

A specific test vehicle has been developed to measure the shear stress–strain hysteresis loop of SAC305 solder joints subjected to thermal cycling. According to Hall’s original work, four strain gages were accurately placed on top/bottom surfaces of the component and the PCB. This study allowed to improve the initial experimentation performed by Hall, which needed two test assemblies to plot one hysteresis loop, whereas only one is required here. Using a specific assembly methodology, microstructure of as-reflowed solder joints was found representative of actual SAC305 interconnects, therefore ensuring a realistic thermomechanical behavior under temperature cycles. Hall’s one-dimensional axisymmetric model was verified comparing the theoretical assembly stiffness parameter with the value measured with the experimental SAC305 shear stress–strain hysteresis loop. The CTE differential between the component and the PCB obtained with the hysteresis loop was also found to be very close to the one optically measured on each part alone. Accelerated thermal cycling test was also conducted and the measured cyclic strain energy density dissipated in SAC305 solder joints was correlated to the number of cycles to failure. Further work is needed to plot other hysteresis curves corresponding to different damage levels (i.e., different temperature cycle amplitudes and/or test assemblies with different constitutive materials that would hopefully allow to cover several orders of magnitude in terms of fatigue criterion and number of cycles to failure) in order to obtain a complete experimental SAC305 fatigue model.

The shear stress–strain hysteresis loop also provides interesting information to determine constitutive laws of solder alloys, which are necessary to accurately perform FEM analysis. The complex material behavior captured during thermal cycling coupled with the use of representative solder interconnects allow the derivation of more accurate elastic, plastic, and viscoplastic models than those obtained with time-consuming and unrealistic tensile, creep, or stress relaxation tests. Using this characterization methodology would represent a non-negligible cost saving for companies whose electronic equipment is mainly used in harsh thermal environments. Moreover, plotting hysteresis loops throughout the entire temperature cycles test could be useful to quantify thermal-induced microstructural evolutions taking place during thermal cycling (i.e., Ag_3Sn IMC coalescence or β -Sn recrystallization for instance). Finally, the experimental procedure described in this paper could also be considered to assess the thermomechanical behavior of any solder compositions if the corresponding solder balls can be supplied.

Acknowledgment

This research work was partially supported by the University of Toulouse and Safran Electronics and Defense. The authors would like to thank N. Da-Silva, S. Martin, A. Jamin, and J. Salmon for their help regarding the test vehicles assembly, as well as J. P. Clech for his insightful comments.

References

- Steinberg, D., 2000, *Vibration Analysis for Electronic Equipment*, 3rd ed., Wiley, New York.
- Fang, L., Bo, J., and Wei, T., 2016, “Review of Board-Level Solder Joint Reliability Under Environmental Stress,” *Prognostics and System Health Management Conference (PHM-Chengdu)*, Chengdu, China, Oct. 19–21, pp. 1–6.
- Lee, W. W., Nguyen, L. T., and Selvaduray, G. S., 2000, “Solder Joint Fatigue Model: Review and Applicability Chip Scale Packages,” *Microelectron. Reliab.*, **40**(2), pp. 231–244.
- Sitaraman, S. K., and Kacker, K., 2005, “Thermomechanical Reliability Prediction of Lead-Free Solder Interconnects,” *Lead-Free Solder: Interconnect Reliability*, D. Shangguan, ed., EDFAS (Electronic Device Failure Analysis Society) and ASM International, Materials Park, OH, pp. 181–198.
- Che, F.-X., Luan, J.-E., Yap, D., Goh, K.-Y., and Baraton, X., 2008, “Thermal Cycling Fatigue Model Development for FBGA Assembly With Sn-Ag-Based Lead-Free Solder,” 33rd IEEE/CPMT International Electronics Manufacturing Technology Conference (IEMT), Penang, Malaysia, Nov. 4–6, pp. 1–6.
- Tsou, C. Y., Chang, T. N., Wu, K. C., Wu, P. L., and Chiang, K. N., 2017, “Reliability Assessment Using Modified Energy Based Model for WLCSF Solder Joints,” *International Conference on Electronics Packaging (ICEP)*, Yamagata, Japan, Apr. 19–22, pp. 7–12.
- Hall, P. M., 1984, “Forces, Moments, and Displacements During Thermal Chamber Cycling of Leadless Ceramic Chip Carriers Soldered to Printed Boards,” *IEEE Trans. Compon. Hybrids, Manuf. Technol.*, **7**(4), pp. 314–327.
- Pao, Y.-H., Badgley, S., Govila, R., Baumgartner, L., Allor, R., and Cooper, R., 1992, “Measurement of Mechanical Behavior of High Lead Lead-Tin Solder Joints Subjected to Thermal Cycling,” *ASME J. Electron. Packag.*, **114**(2), pp. 135–144.
- Jih, E., and Pao, Y.-H., 1995, “Evaluation of Design Parameters for Leadless Chip Resistors Solder Joints,” *ASME J. Electron. Packag.*, **117**(2), pp. 94–99.
- Clech, J.-P., 1997, “Solder Reliability Solutions: A PC-Based Design-for-Reliability Tool,” *Soldering Surf. Mount Technol.*, **9**(2), pp. 45–54.
- Clech, J.-P., 2018, “Chapter 2: Solder Properties, Joint Mechanics, Fatigue and Failure,” EPISI, accessed Feb. 2, 2019, www.msed.nist.gov/solder/clech/Sn-Pb_Creep.htm
- Fan, X. J., Varia, B., and Han, Q., 2010, “Design and Optimization of Thermo-Mechanical Reliability in Wafer Level Packaging,” *Microelectron. Reliab.*, **50**(4), pp. 536–546.
- Young, W. C., and Budynas, R. G., 2002, *Roark’s Formulas for Stress and Strain*, McGraw-Hill, New York.
- Vishay Precision Group, 2010, “Strain Gage Adhesives,” Vishay Precision Group, Malvern, PA, accessed Feb. 23, 2010, www.dmesures.fr/images/FT_jauges_accessoires/dtcolles.pdf
- Zhang, Y., Zhu, H., Fujiwara, M., Xu, J., and Dao, M., 2013, “Low-Temperature Creep of SnPb and SnAgCu Solder Alloys and Reliability Prediction in Electronic Packaging Modules,” *Scr. Mater.*, **68**(8), pp. 607–610.
- Arfaei, B., Wentlent, L., Joshi, S., Alazzam, A., Tashoutsh, T., Halaweh, M., Chivukula, S., Yin, L., Meilunas, M., Cotts, E., and Borgesen, P., 2012, “Improving the Thermomechanical Behavior of Lead Free Solder Joints by Controlling the Microstructure,” 13th InterSociety Conference on Thermal and Thermomechanical Phenomena in Electronic Systems, San Diego, CA, May 30–June 1, pp. 392–398.
- Choubey, A., 2007, “Microstructural Changes Under Isothermal Aging and Their Influence on Thermal Fatigue Reliability for Tin-Lead and Lead-Free Solder Joints, Including Microstructural Changes Under Isothermal Aging in Mixed Solder Joints,” *Ph.D. thesis*, University of Maryland, College Park, MD.
- IPC, 2006, “Performance Tests Methods and Qualification Requirements for Surface Mount Solder Attachments,” Association Connecting Electronics Industries, Bannockburn, IL, Standard No. IPC-9701A.
- Cadek, J., 1988, “Creep in Metallic Materials,” *Materials Science Monographs*, Vol. 48, Elsevier, Amsterdam, The Netherlands.
- Hall, P. M., 1987, “Creep and Stress Relaxation in Solder Joints of Surface-Mounted Chip Carriers,” *IEEE Trans. Compon. Hybrids, Manuf. Technol.*, **12**(4), pp. 556–565.
- Yin, L., Wentlent, L., Yang, L., Arfei, B., Osaimieh, A., and Borgesen, P., 2012, “Recrystallization and Precipitate Coarsening in Pb-Free Solder Joints During Thermomechanical Fatigue,” *J. Electron. Mater.*, **41**(2), pp. 241–252.
- Holderlann, K., Cuddalorepatta, G., and Dasgupta, A., 2008, “Dynamic Recrystallization of Sn3.0Ag0.5Cu Pb-Free Solder Alloy,” *ASME Paper No. IMECE2008-67671*.
- Yao, Y., Long, X., and Keer, L. M., 2017, “A Review of Recent Research on the Mechanical Behavior of Lead-Free Solders,” *Appl. Mech. Rev.*, **69**(4), pp. 1–15.
- Zhang, Q., Dasgupta, A., Nelson, D., and Pallavicini, H., 2005, “Systematic Study on Thermo-Mechanical Durability of Pb-Free Assemblies: Experiments and FE Analysis,” *ASME J. Electron. Packag.*, **127**(4), pp. 415–429.
- Ladani, L. J., 2010, “Successive Softening and Cyclic Damage in Viscoplastic Material,” *ASME J. Electron. Packag.*, **132**(4), pp. 1–7.
- Ridout, S., and Bailey, C., 2006, “Review of Methods to Predict Solder Joint Reliability Under Thermo-Mechanical Cycling,” *Fract. Fatigue Eng. Mater. Struct.*, **30**(5), pp. 400–412.
- Pang, J. H. L., Tan, T. I., and Sitaraman, S. K., 2002, “Thermo-Mechanical Analysis of Solder Joint Fatigue and Creep in a Flip Chip on Board Package Subjected to Temperature Cycling Loading,” 48th Electronic Components and Technology Conference, Seattle, WA, Aug. 6, pp. 878–883.